Imaging mantle structure using stacking and migration techniques

John Woodhouse

SPICE workshop, Cargèse, May 2007

Collaborators

Kit Chambers

Arwen Deuss

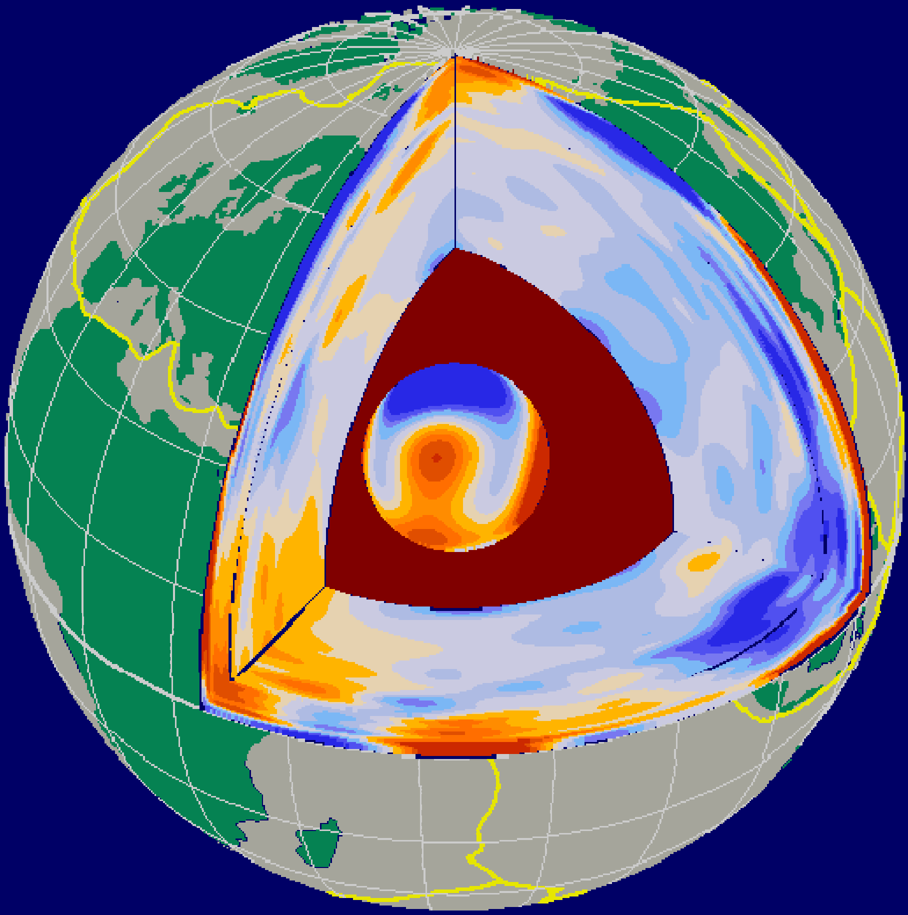

Model S20RTS: Ritsema, van Heijst and Woodhouse 1999,2004

Resolution kernels for $\delta \ln(v_s)$ in model S20RTS

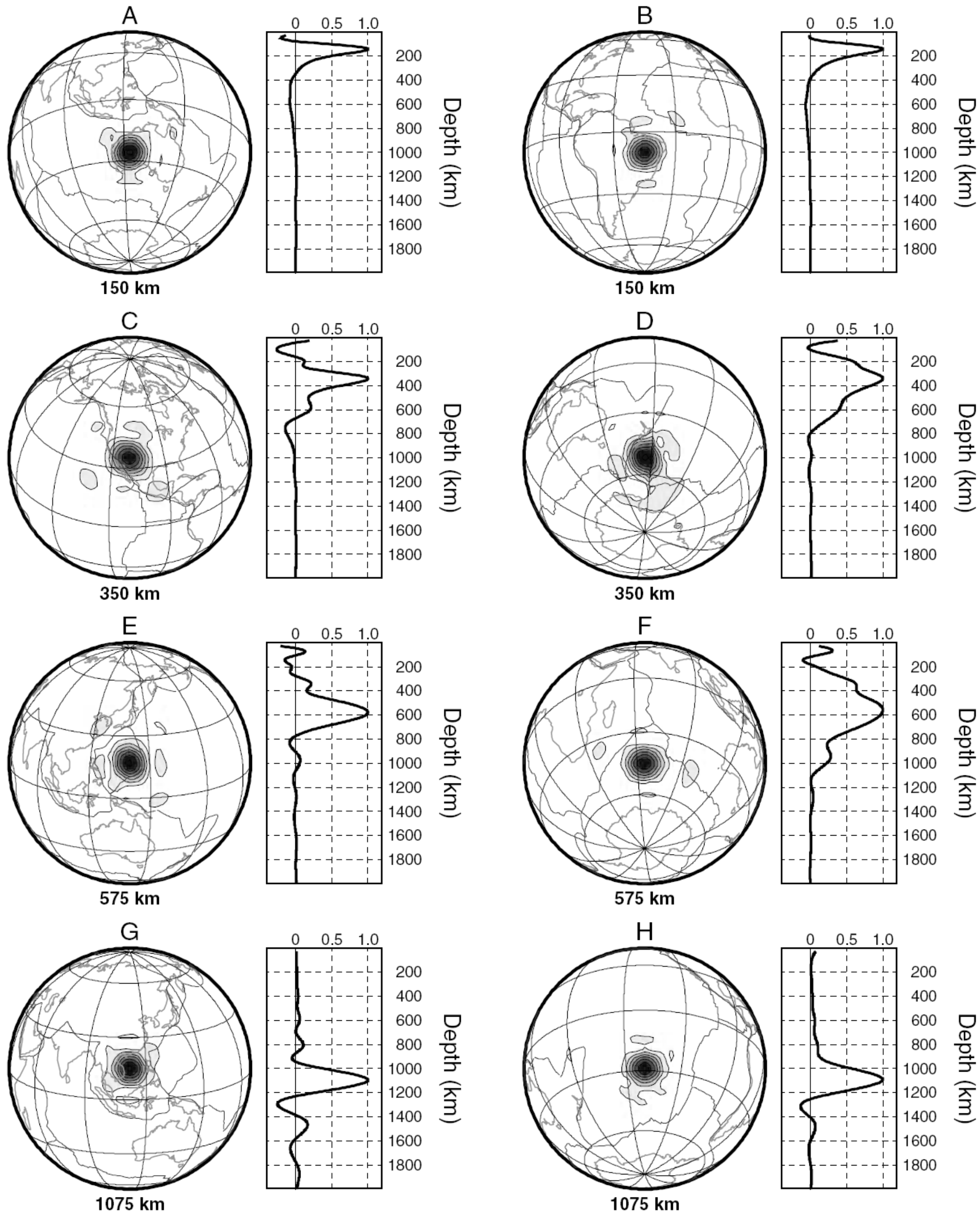

Ritsema, van Heijst and Woodhouse, JGR, 2004

SS-precursors

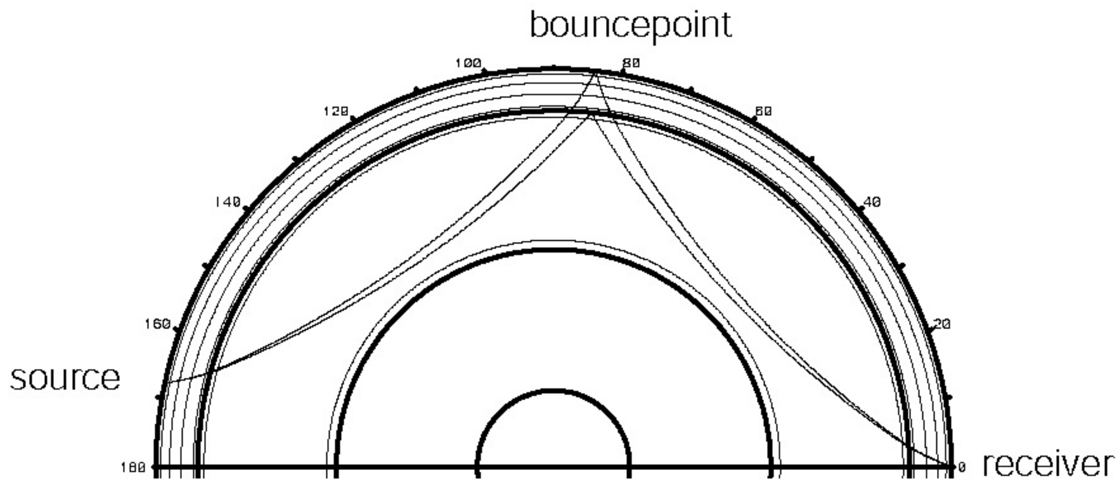

Detection of mantle discontinuities

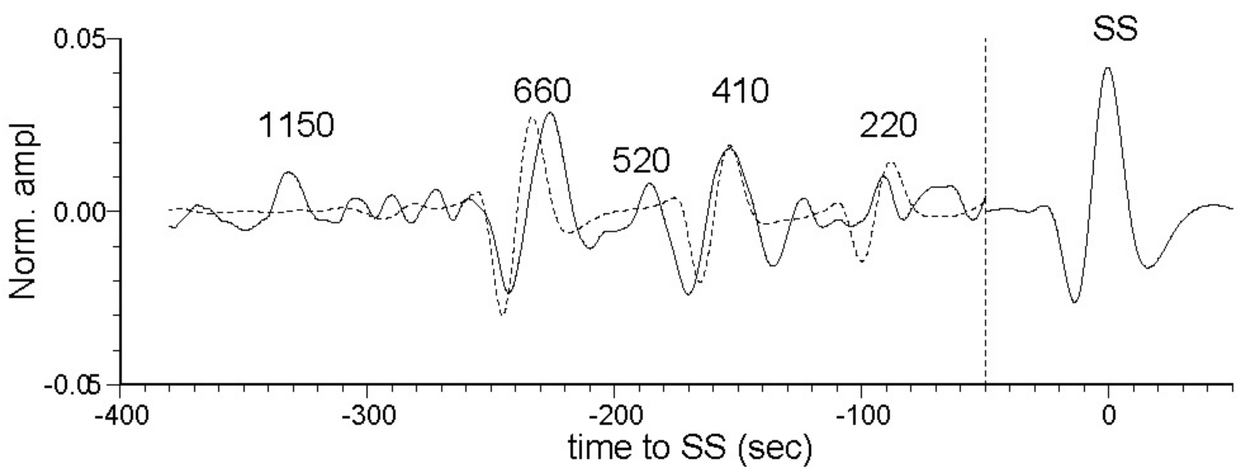

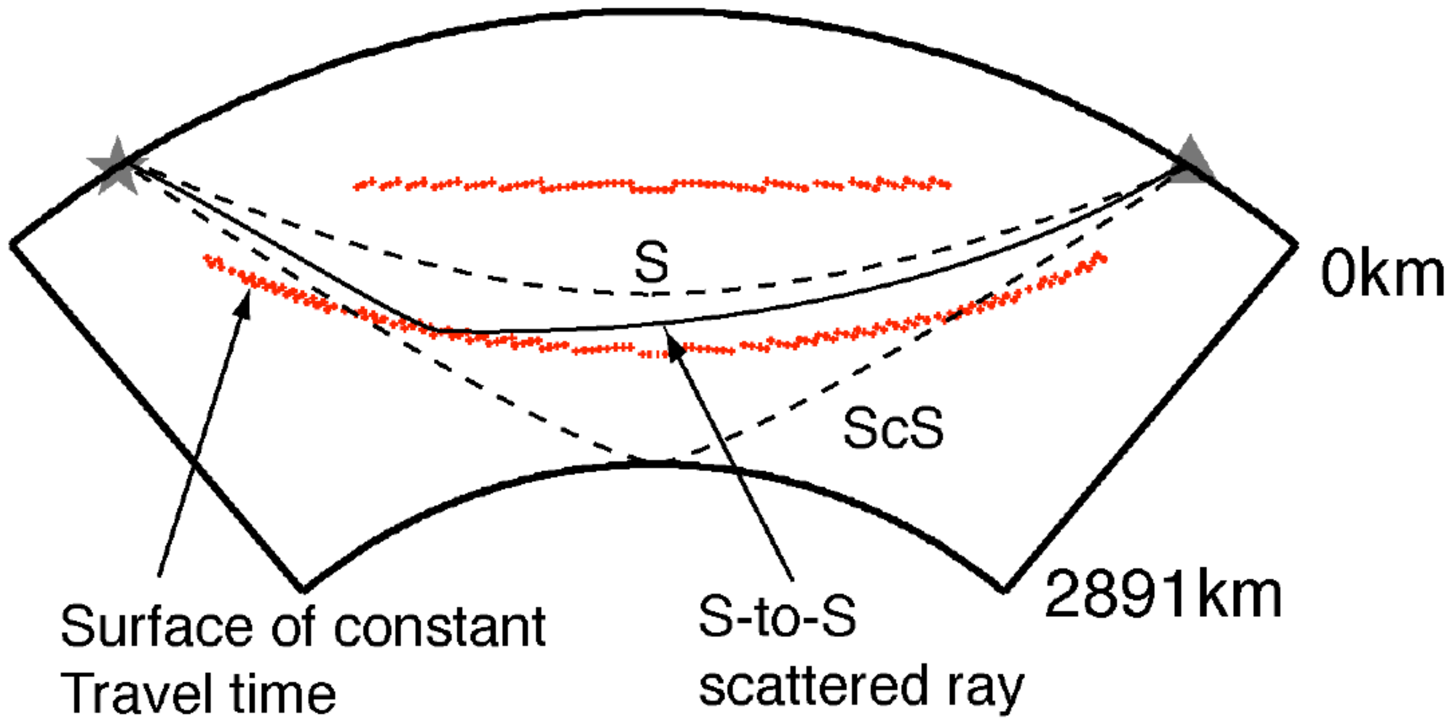

S-to-S scattering geometry. Each time sample is considered a sum of contibutions from a surface of constant travel time.

Robustness of reflections
Deep reflectors in North America

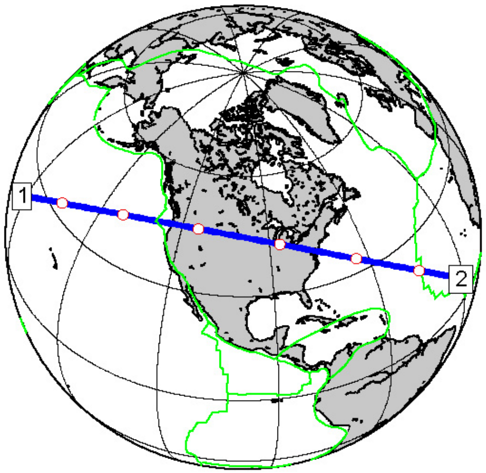

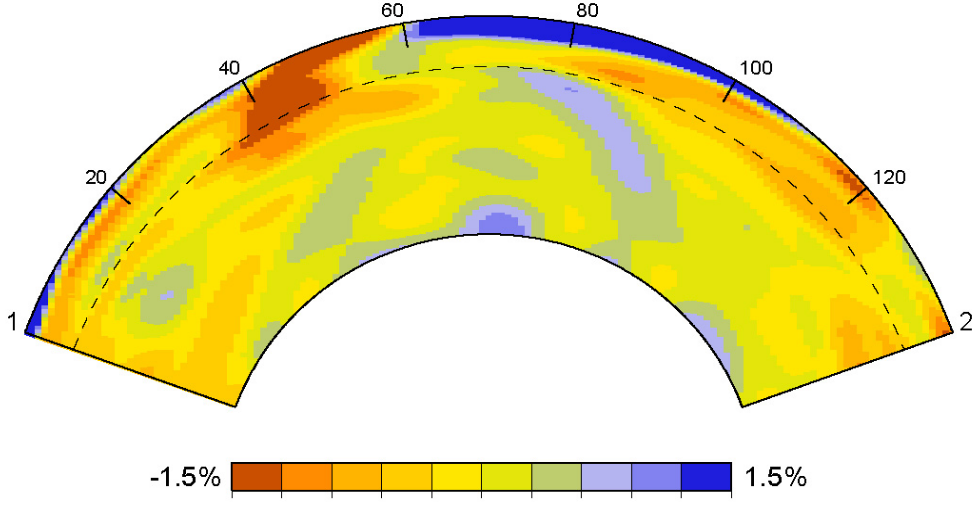

Stack for North America

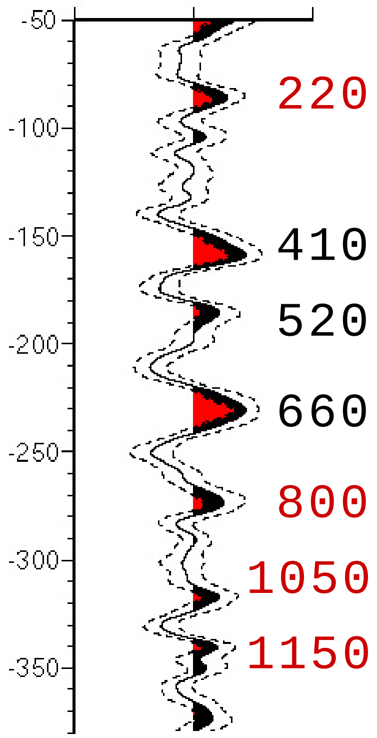

Deep reflectors in Indonesia

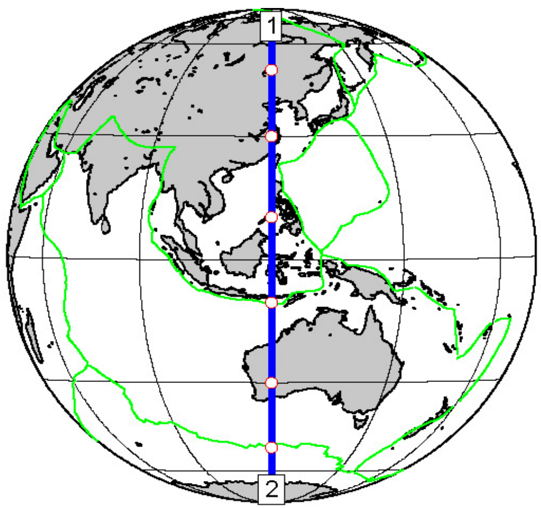

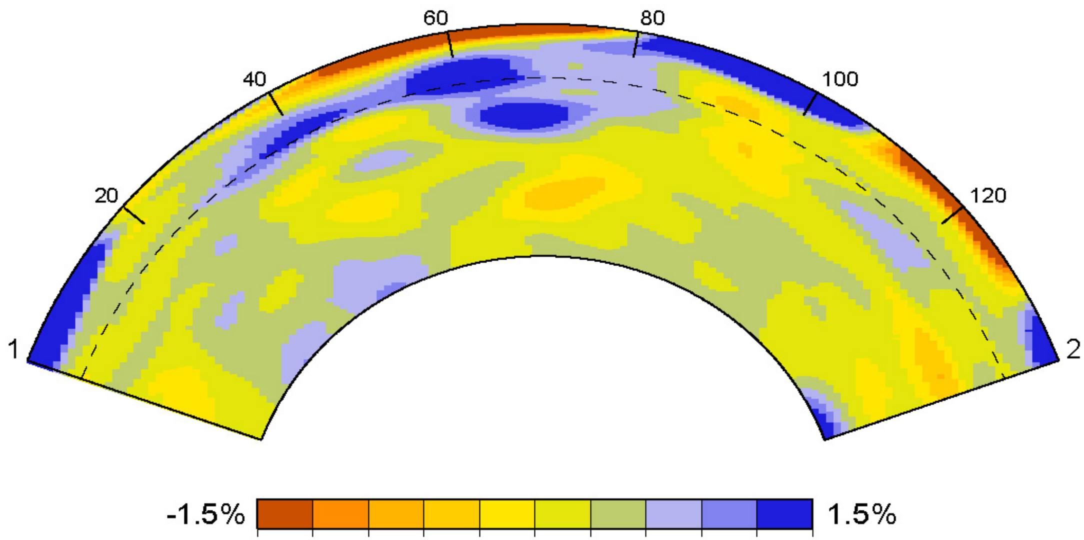

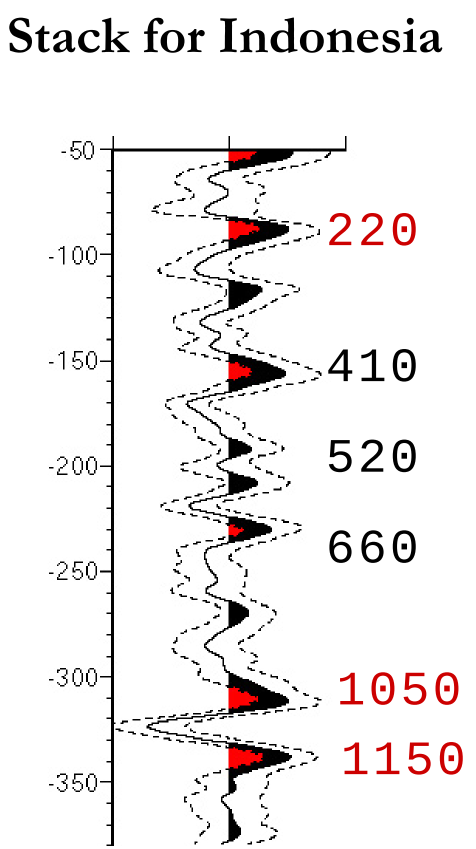

[*Deuss, DPhil Thesis 2002*]

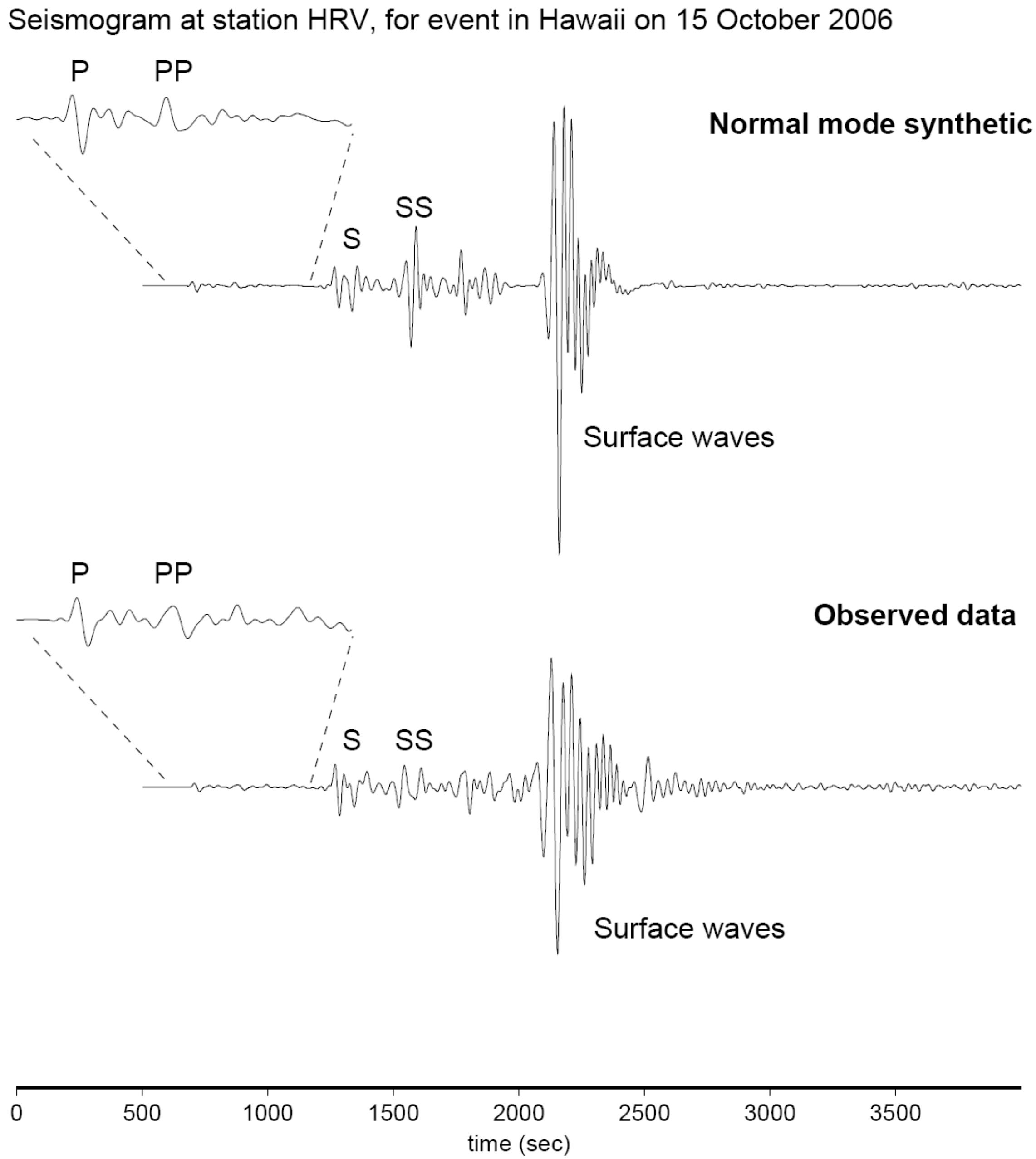

Figure 2: Data and synthetic for a vertical component record at station HRV following the recent event in Hawaii on 15 October 2006. The epicentral is 73°. For the calculation of the synthetic seismogram the Harvard/Lamont quick-CMT centroid location and moment tensor parameters were used (G. Ekström, www.globalcmt.org).

Examples of data and (PREM) synthetic seismograms

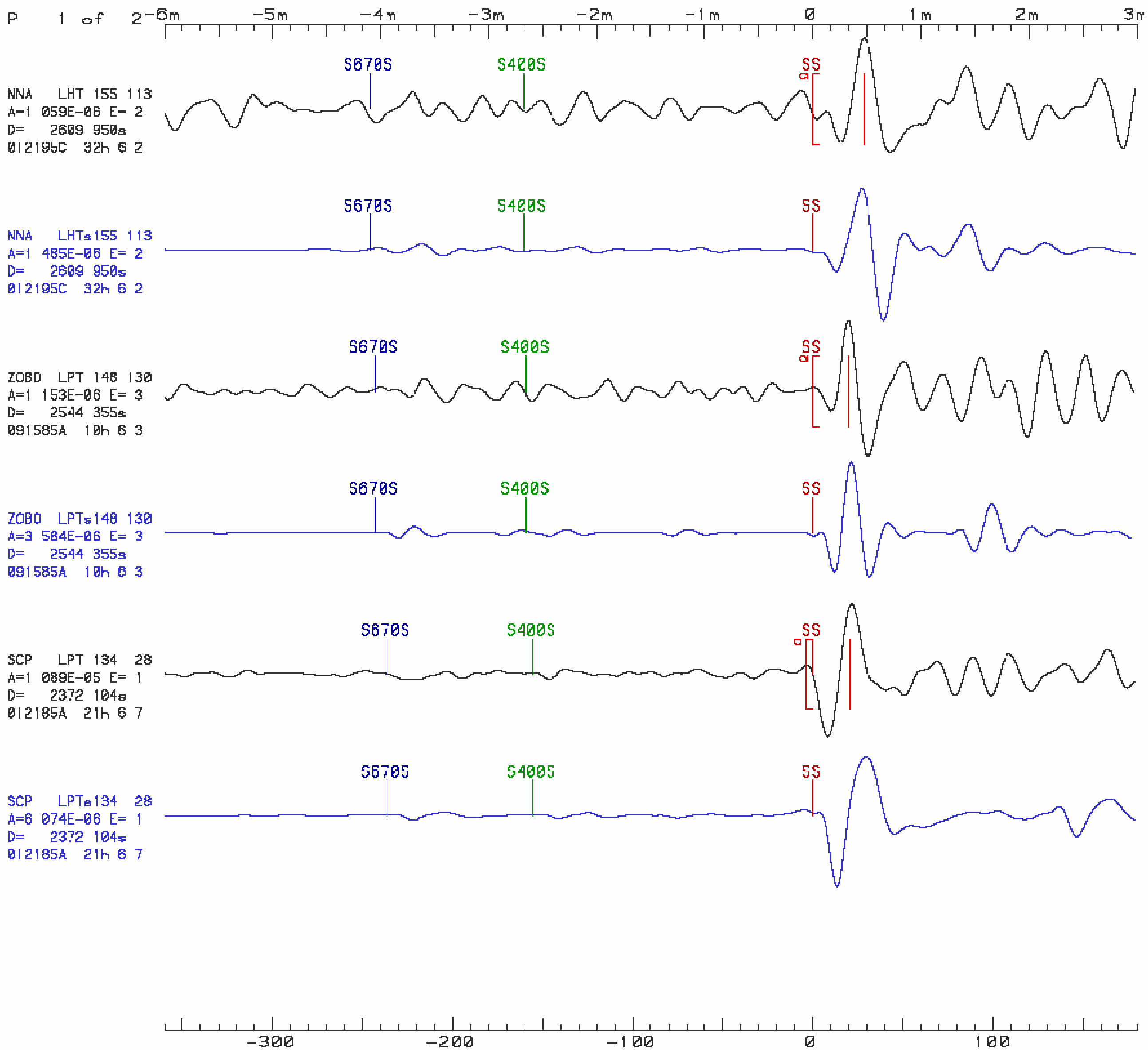

Examples of selected data traces (black lines) and corresponding synthetic traces computed for PREM (blue lines). The data is lined up for SS; the SS phase and its precursors S400S and S670S are named and the red brackets and 'a' denote the picked SS phase.

Lateral variations in discontinuity depths determined using the P410P and S410S datasets using different scaling factors for the (S20RTS) travel time correction. The maps were derived by multiplying the normal (scale factor of 1.0) travel time corrections before applying these to the measured P410P − PP and S410S −SS lag times and converting these to discontinuity depths.

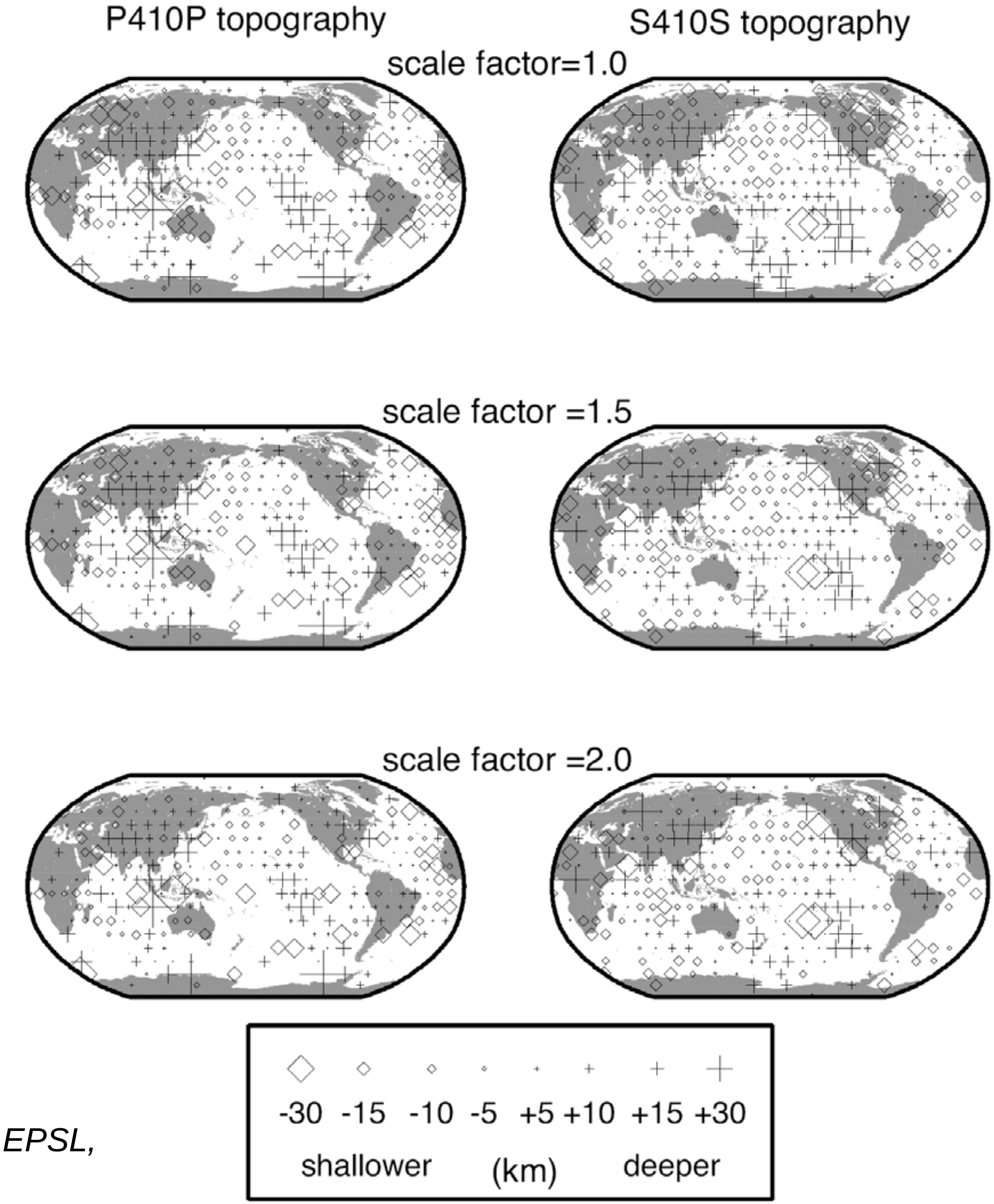

Chambers, Woodhouse, Deuss, EPSL, 2005

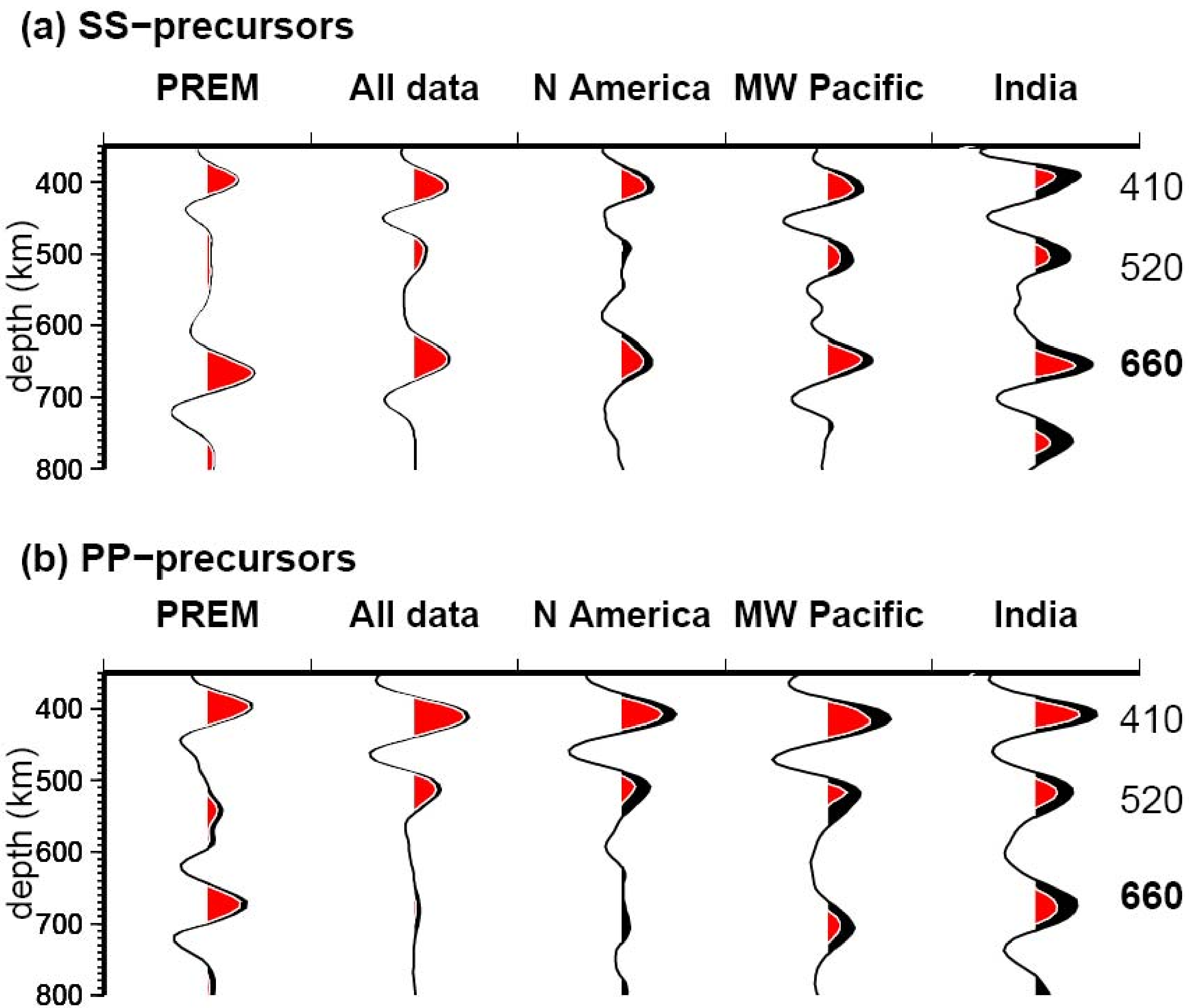

Stacked traces for synthetic and real data North America (484 traces), the Mid West Pacific (808 traces) and India (272 traces). The depths are corrected fo crustal and mantle structure using CRUST5.1 and S20RTS.

Deuss, Redfern, Chambers, Woodhouse, Science, *2006*

Stacked traces for PP and SS precursors for several cross sections in the northern hemisphere.
Blue boxes denote areas where robust reflections from the 660 km discontinuity are seen in PP precursors. For some stacks, the relative amplitude between P410P and P660P is similar to the ratio for SS precursors.

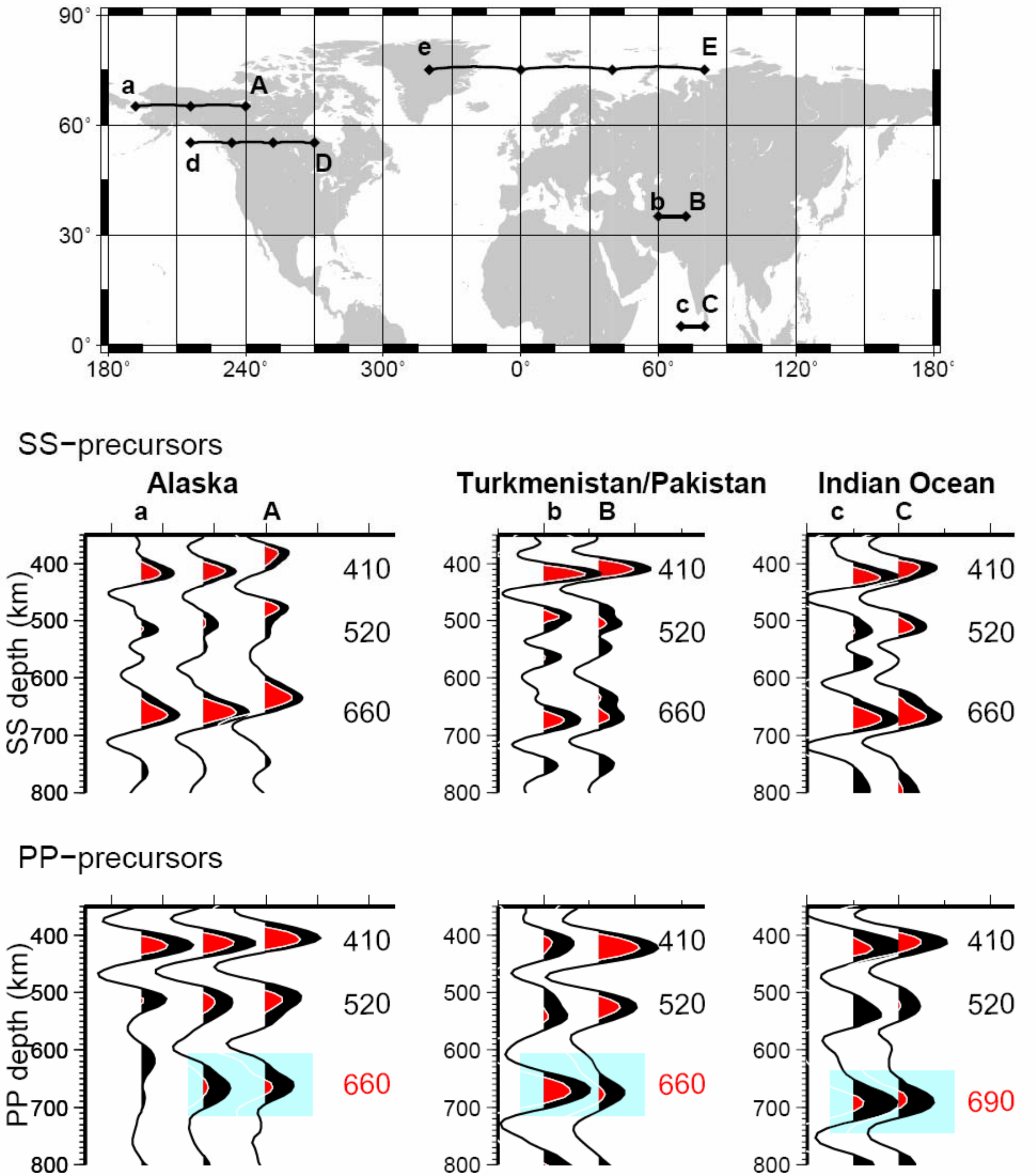

Deuss, Redfern, Chambers, Woodhouse, Science, *2006*

PP precursor observations in two different frequency bands.

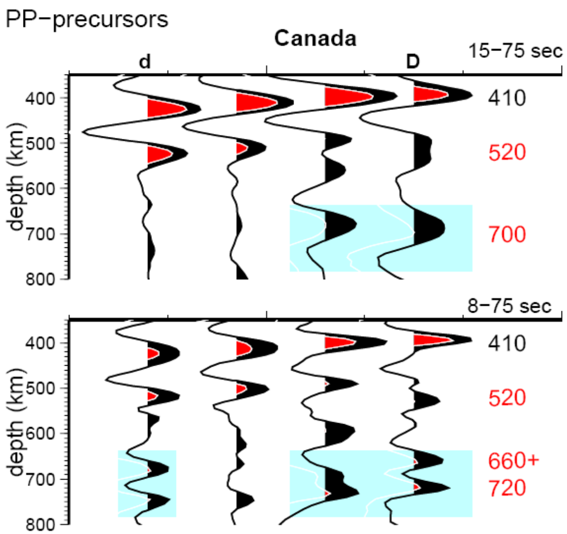

15-75s band

8-75s band

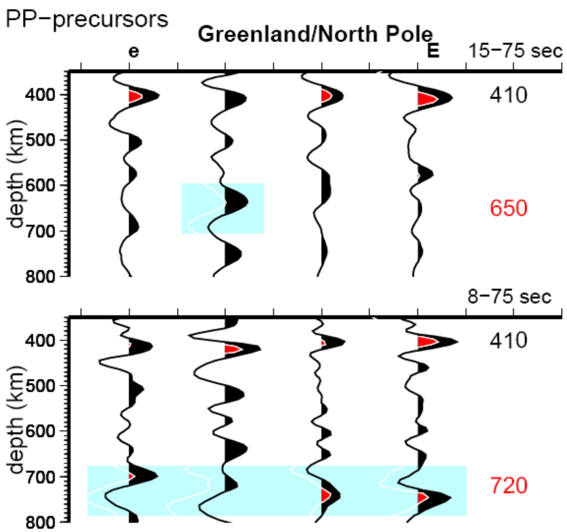

15-75s band

8-75s band

.Deuss, Redfern, Chambers, Woodhouse, Science, *2006*

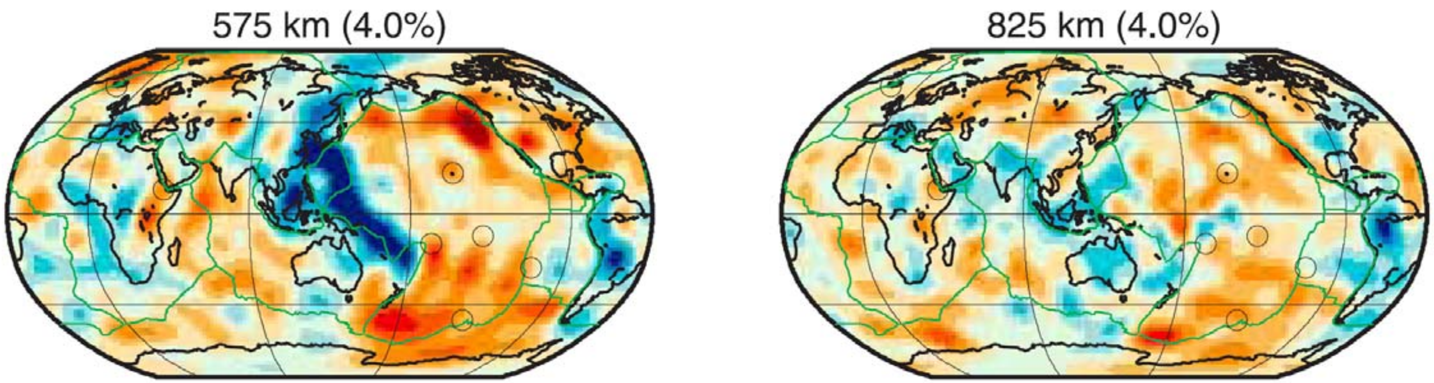

S20RTS

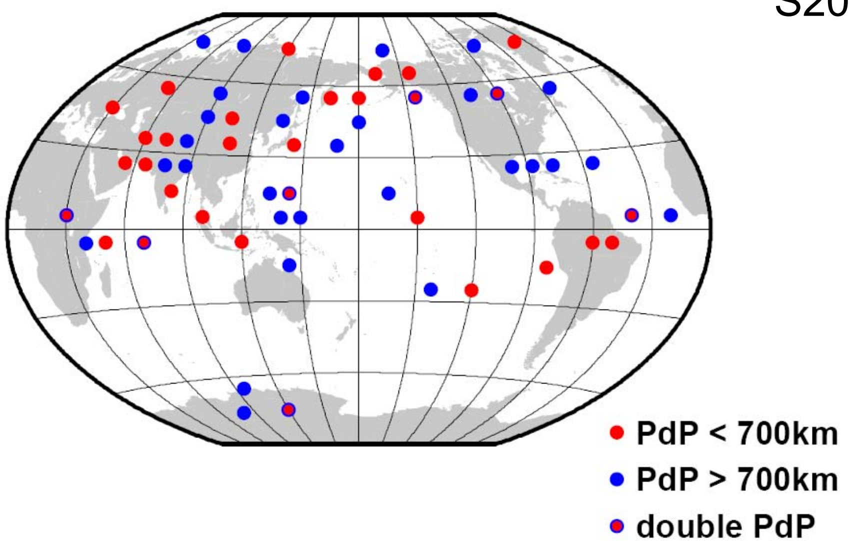

Overview where reflections from the 660 km discontinuity are found in the 8-75sec frequency band.

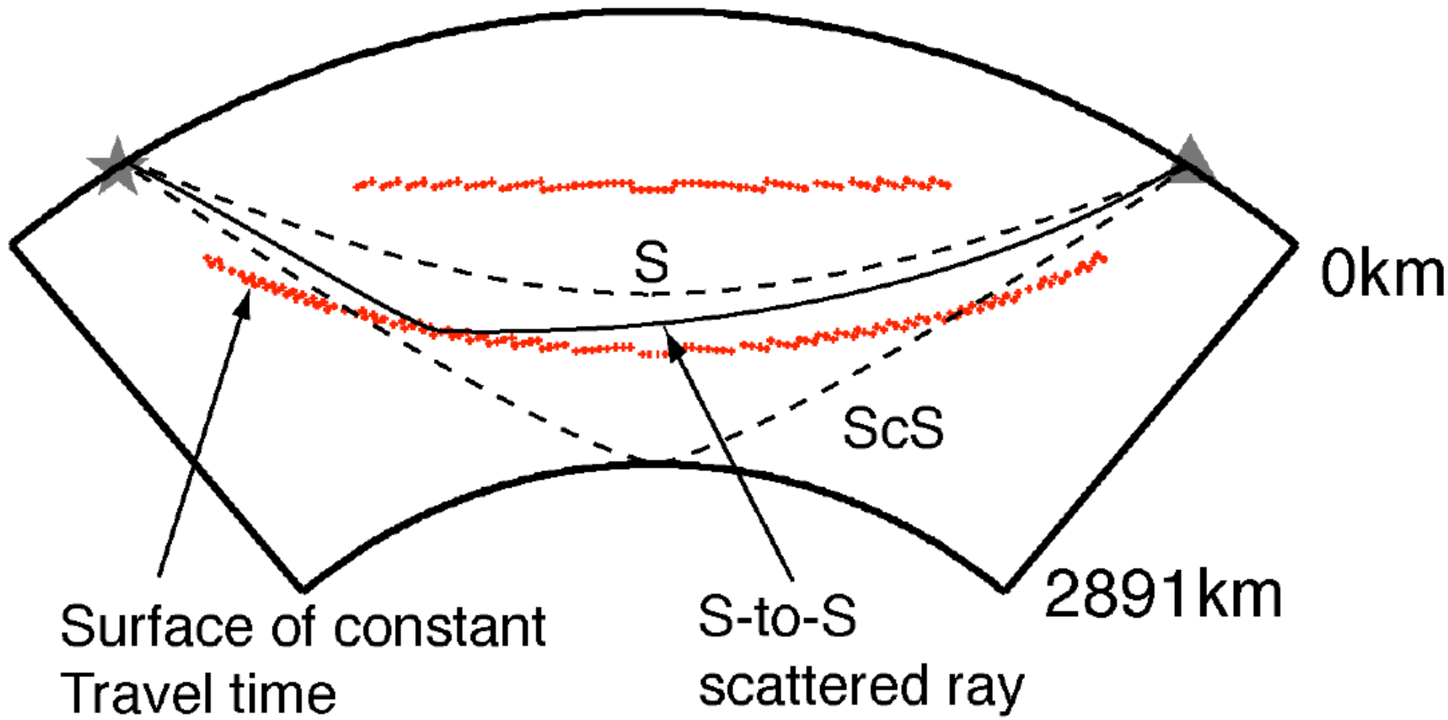

S-to-S scattering geometry. Each time sample is considered a sum of contibutions from a surface of constant travel time.

Single scattering approximation

Starting from the elastodynamic equations in a homogeneous medium:

$$\rho u_{i,tt} - \big(\mu(u_{i,j} + u_{j,i}) + \lambda u_{k,k}\delta_{ij}\big)_{,j} = f_i$$

u_i	elastic displacement field
λ, μ	elastic parameters
ρ	density

Perturbing the medium $\mu \to \mu + \delta\mu(\mathbf{x})$ etc. we obtain the linearized equation for the scattered field δu_i:

$$\rho\, \delta u_{i,tt} - \big(\mu(\delta u_{i,j} + \delta u_{j,i}) + \lambda\, \delta u_{k,k}\delta_{ij}\big)_{,j} = -\delta\rho\, u_{i,tt} + \big(\delta\mu(u_{i,j} + u_{j,i}) + \delta\lambda\, u_{k,k}\delta_{ij}\big)_{,j} \equiv f_i(\mathbf{x}, t)$$

This enables the 'single scattered' field to be evaluated using the Green's function for the homogeneous medium.

$$\delta u_i = \int G_{ik}(\mathbf{x}, t, \mathbf{x}', t') f_k(\mathbf{x}', t')\, \mathrm{d}^3x'\, \mathrm{d}t'$$

Migration/Inversion via the generalized Radon Transform

Forward model for the scattered wavefield

$$u_i(\mathbf{r},\mathbf{s},\omega) = \frac{\omega^2}{4\pi}\int \frac{R_s(\mathbf{s},\mathbf{x},\mathbf{r})}{\beta(\mathbf{x})^2}\left[2A_i(\mathbf{s},\mathbf{x},\mathbf{r}) + (2+\kappa)\,B_i(\mathbf{s},\mathbf{x},\mathbf{r})\right] \times \frac{\delta\beta}{\beta}(\mathbf{x})\exp\left[-i\omega\tau(\mathbf{s},\mathbf{x},\mathbf{r})\right] d^3\mathbf{x}$$

Based upon the Born approximation (single-scattering) and ray theoretical Greens functions the scattered wavefield, u_i, is considered a sum of contributions from point scatterers with velocity anomaly, $\delta\beta/\beta$. The contribution from each point scatterer is weighted by the geometrical spreading, R_S, and radiation patterns associated with the source-scatterer receiver path, A_i and B_i. The latter are given by:

$$A_i = \left(\delta_{ik} - \frac{x_i x_k}{r^2}\right)\hat{\alpha}_k, \quad B_i = \left(\delta_{i1}\frac{x_k}{r} + \delta_{ik}\frac{x_1}{r} - \frac{2x_i x_k x_1}{r^3}\right)\hat{\alpha}_k, \quad \frac{\delta\rho}{\rho} = \kappa\frac{\delta\beta}{\beta}$$

where the components (x_1,x_2,x_3) refer to the orientation of the scattered ray relative to an incident ray traveling in the x_1 direction and the S-wave polarization is given by components α_k. In order to make the scattered wavefield the sum of a single scattering potential, the radiation patterns for velocity and density are related by a constant, κ, (0.3).

Since here we are concerned with S-waves in the ray approximation, we use the far-field S-wave part of the Green's function

$$G_{ik}(\mathbf{x}, t, \mathbf{x}', t') \sim \frac{1}{4\pi\mu|\mathbf{x} - \mathbf{x}'|} \left(\delta_{ik} - \frac{(x_i - x_i')(x_k - x_k')}{|\mathbf{x} - \mathbf{x}'|^2} \right) \delta(t - t' - |\mathbf{x} - \mathbf{x}'|/\beta)$$

which can be used to derive the radiation pattern and polarization of the S-waves generated by 'point scatterers'.

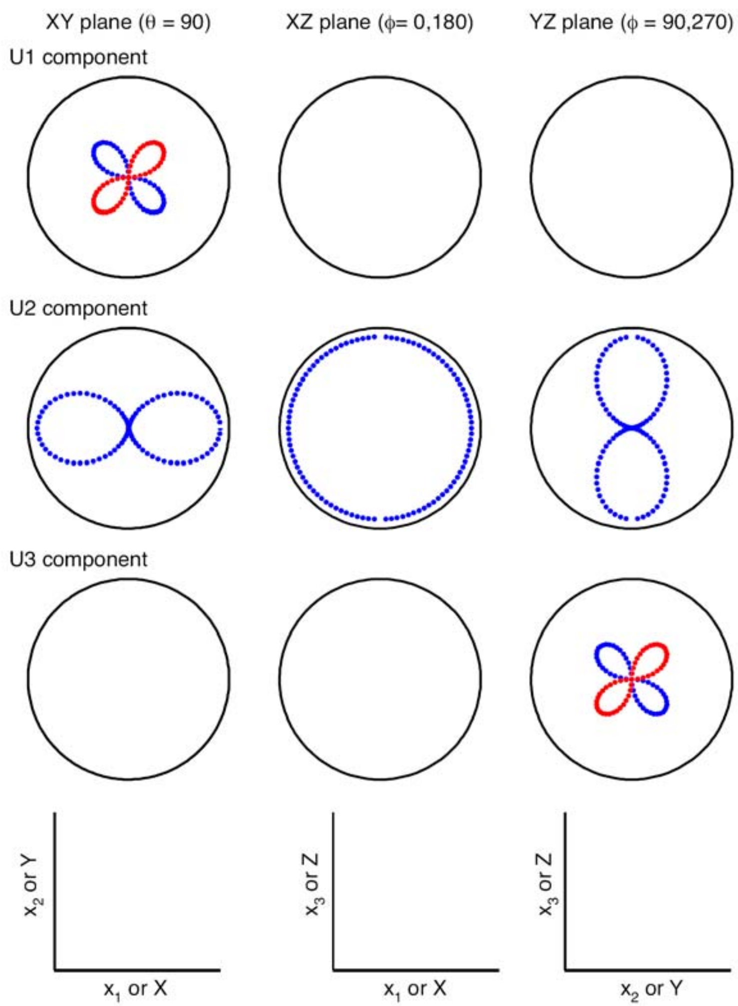

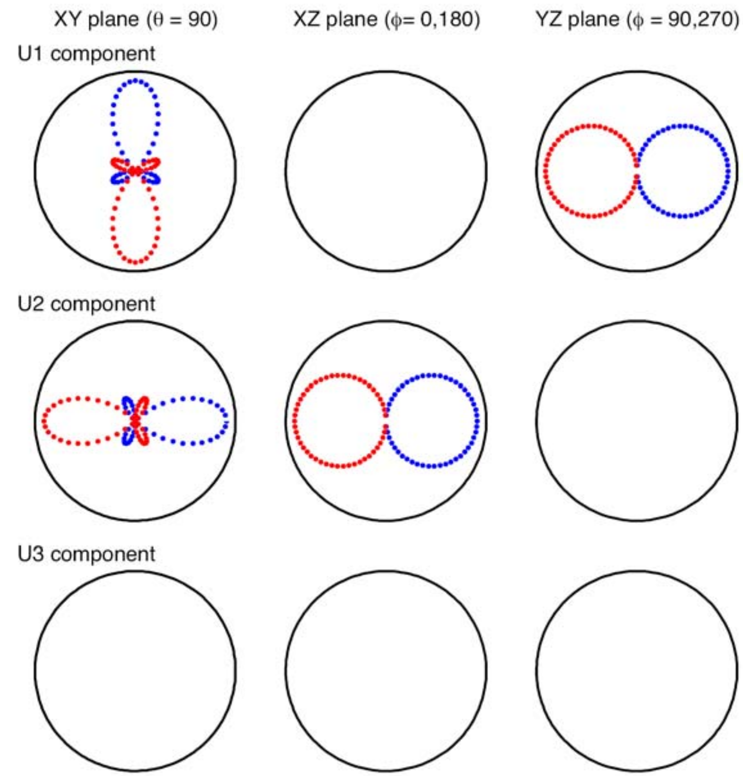

Migration/Inversion via the generalized Radon Transform

Migration/Inversion procedure

$$\langle \frac{\delta\beta}{\beta}(\mathbf{x_0})\rangle = \frac{1}{\pi^2}\int \frac{\left|\cos\alpha(\mathbf{r},\mathbf{x_0},\mathbf{s})\right|^3}{\beta(\mathbf{x_0})^3}\frac{1}{\Gamma'(\mathbf{r},\mathbf{x_0},\mathbf{s})R_s(\mathbf{r},\mathbf{x_0},\mathbf{s})}$$
$$\times u\left(\mathbf{r},\mathbf{s},t=\tau(\mathbf{r},\mathbf{x_0},\mathbf{s})\right)d^2\boldsymbol{\xi}(\mathbf{r},\mathbf{x_0},\mathbf{s})$$

The migration/inversion scheme is based on that of Miller et. al. (1987). Figure 1 shows how the scattering half angle α, and unit normal, ξ, relate to the source receiver geometry.

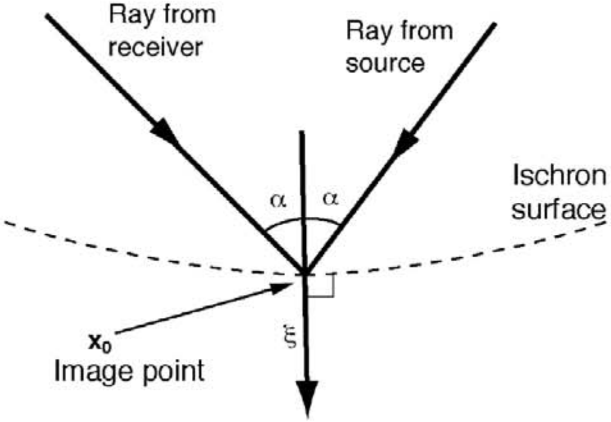

Figure 2 - Definition of symbols in migration scheme.

Nulls resulting from the source and scatterer radiation patterns will amplify low amplitude traces in the stacking process. Accordingly we damp the contribution from geometries near radiation pattern nodes using:

$$\frac{1}{\Gamma'} = \begin{cases} 1/\Gamma & |\Gamma| \geq \sigma \\ (\Gamma/\sigma^2)\exp\left[1-(\Gamma/\sigma)^2\right] & |\Gamma| < \sigma \end{cases}$$

$$\Gamma(\mathbf{r},\mathbf{x_0},\mathbf{s}) = \left(2\left(A_i+B_i\right)+\kappa B_i\right)\epsilon_i$$

where ε_i is the transverse polaristaion vector. Testing showed stable results were obtained using $\sigma = 0.5$.

Phase stripping technique (Kendall and Shearer, 1995)

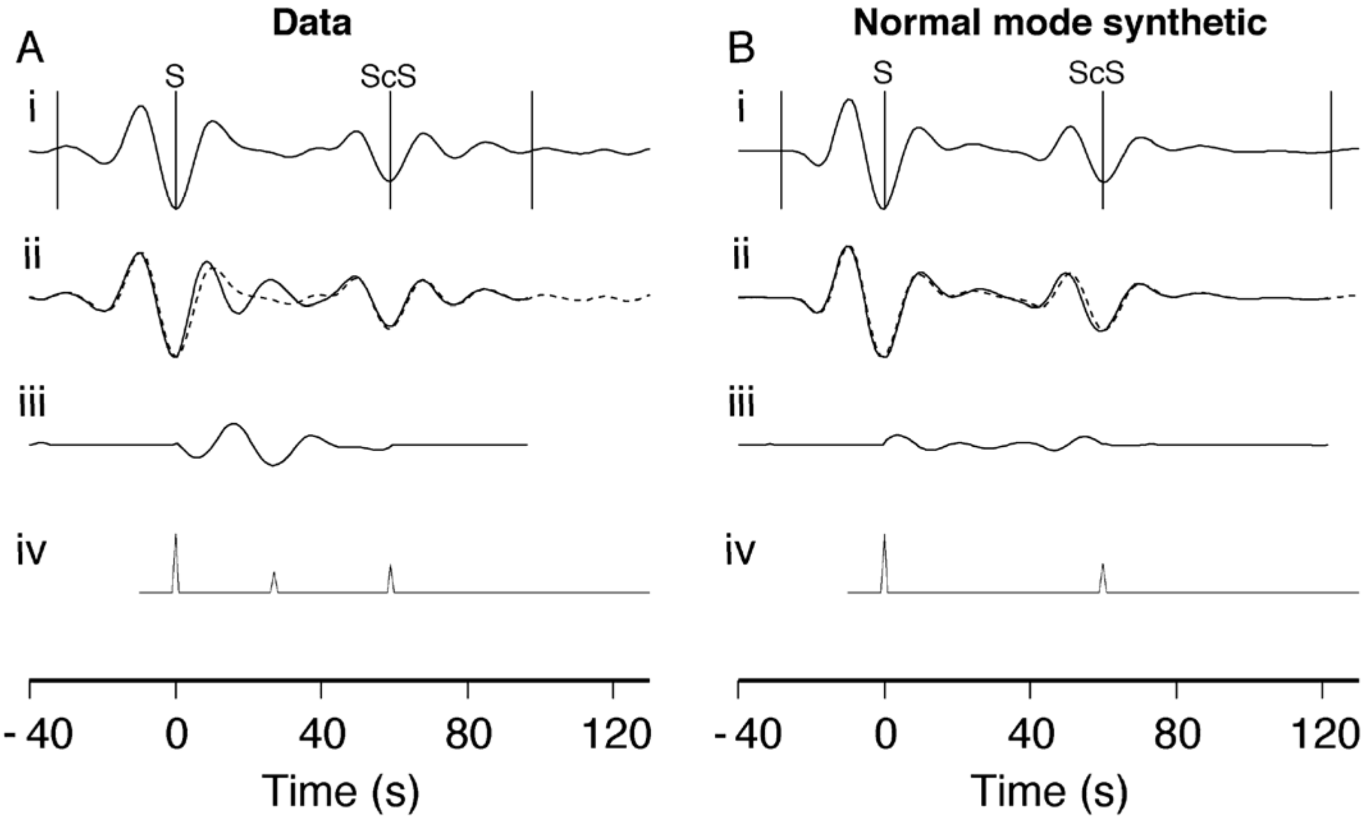

1 - The start of the S phase and finish of ScS were hand picked in 1075 traces (i)
2 - The picked portions of S and ScS were placed together to form a reference pulse.
3 - A reference trace is made by placing the reference pulse at the position of the S and ScS arrivals. In (ii) the reference trace (solid) is overlain on the original data (dashed).
4 - The reference trace is subtracted from the data to a residual or phase stripped trace (iii). The phase stripped trace were used as the data for the GRT migration/inversion.
5 - Spikes were progressively fit to the phase stripped traces to form spike sequences (iv). These were used as data for the initial backprojection.

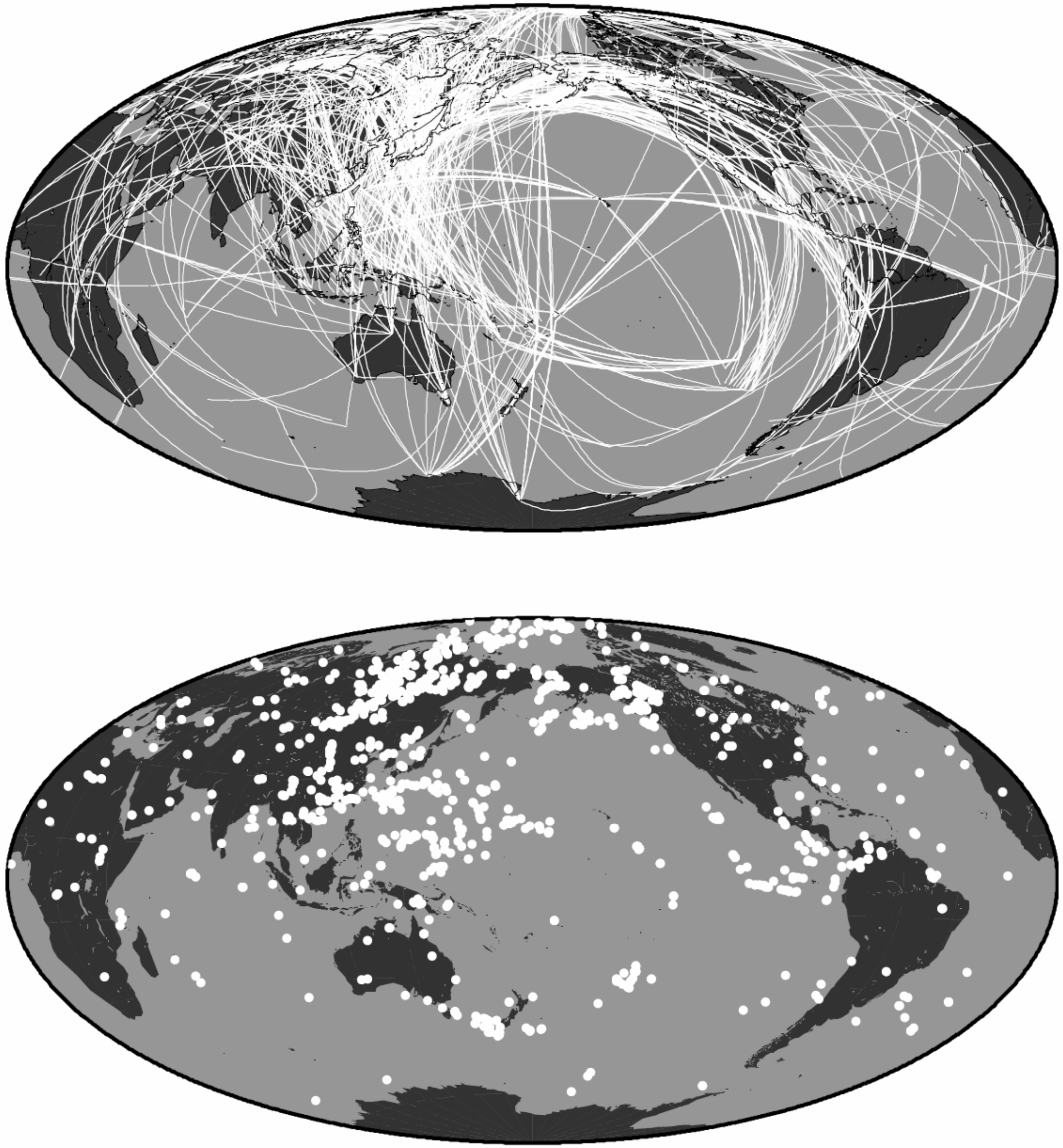

(top) Source receiver paths for the dataset of phase striped traces. (Bottom) global distribution of source-receiver mid-points.

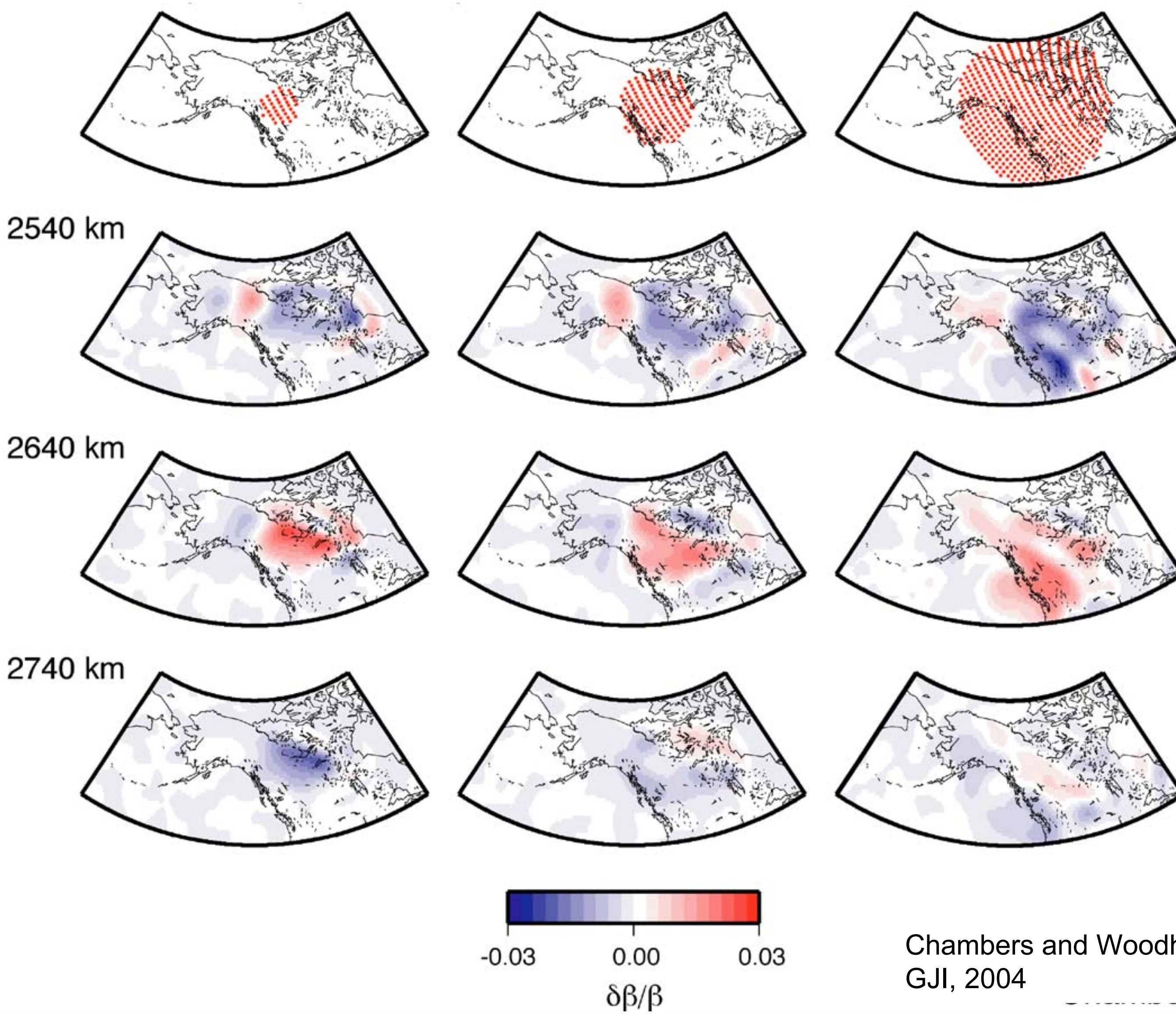

Chambers and Woodhouse,
GJI, 2004

Synthetic resolution tests. Synthetics were made using the forward model for the scattered wavefield (see above) and discs made up of point scatterers at 2640km depth. The synthetics were then subjected to the same migration procedure as the data. For the largest disc positive velocities are retreived beneath much of Alaska, and in the North Pacific. This is not seen in the data and suggests the D'' discontinuity is limited to the area near the Canadian border.

Results from the Generalized Radon Transform stack and synthetic stacks based on simple structures

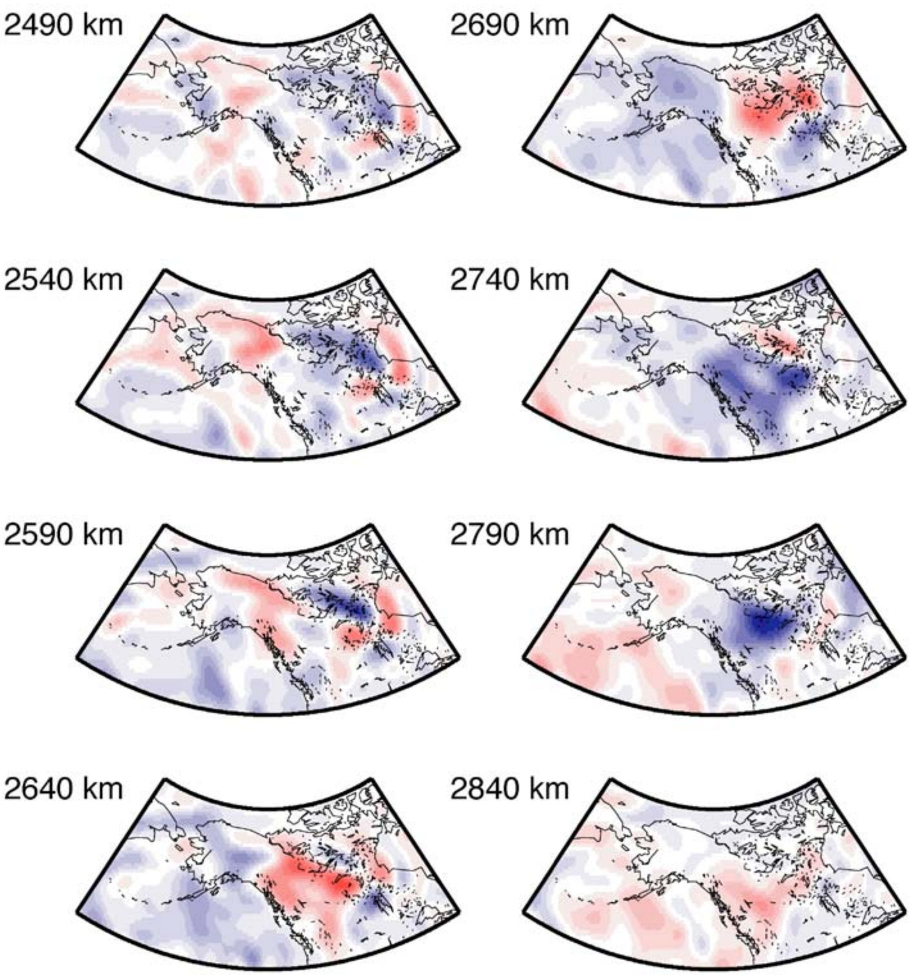

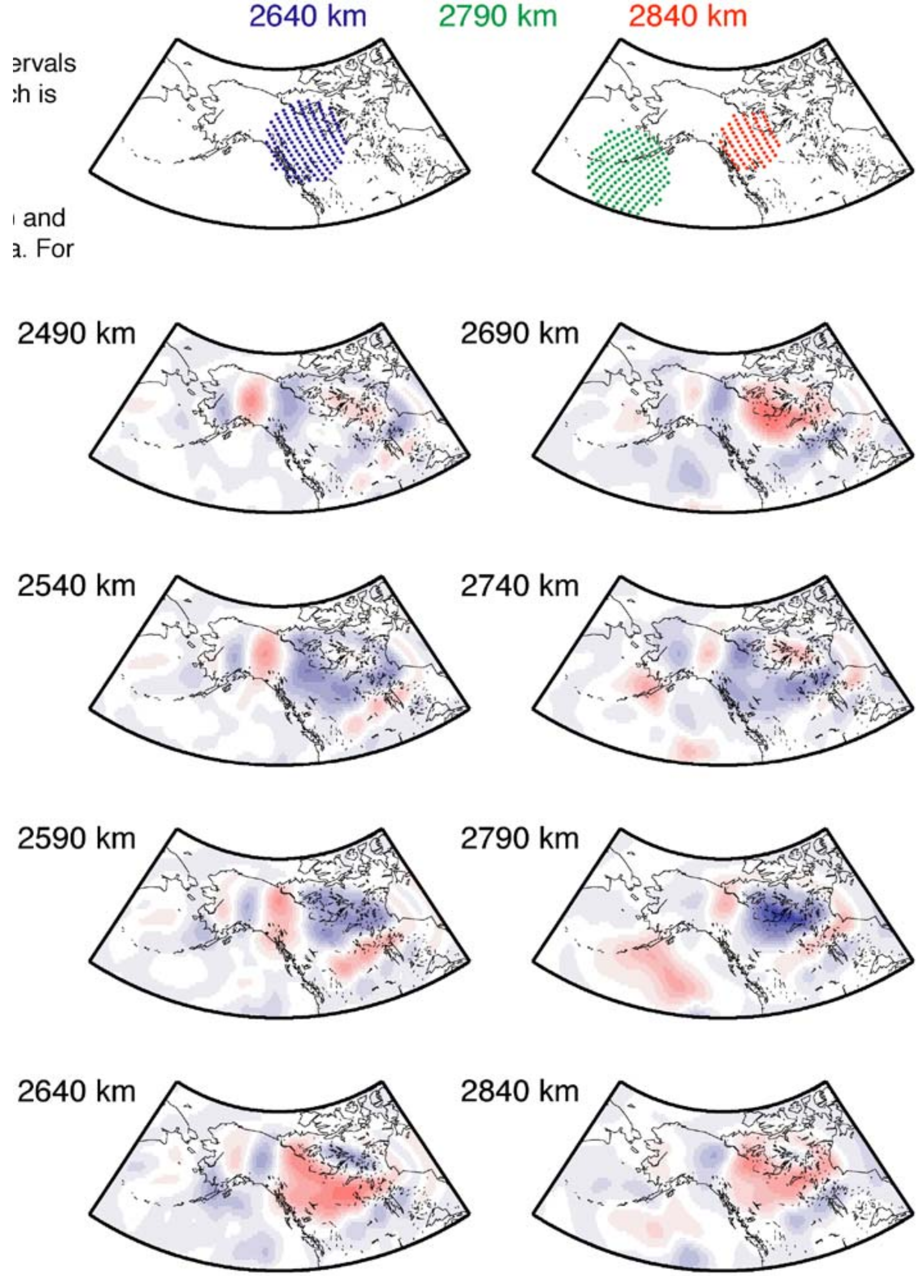

GRT Migration results for North Central Asia

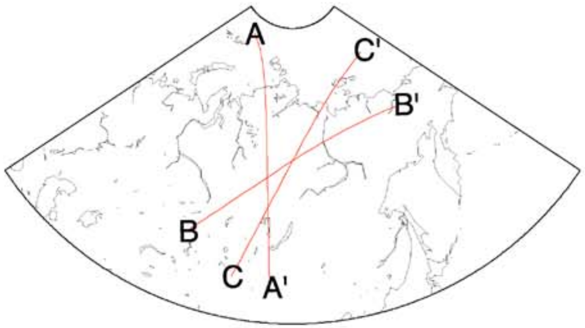

Cross section views through the migration results **(a)** and synthetic tests **(b & c)**. Each section has a length of 40^{o}. The positive anomaly near the centre of each plot is the D" reflector, arrows marked the postion where this stops.

In the synthetic tests **(b & c)** black dots show the position of input point scatterers. These show that the D" reflector is resolvable in the marked regions, where it is absent from the data. The absence of the D" reflector can't be attributed to topography or focussing effects (c), instead it requires lateral variation in the impedance contrast across the discontinuity.

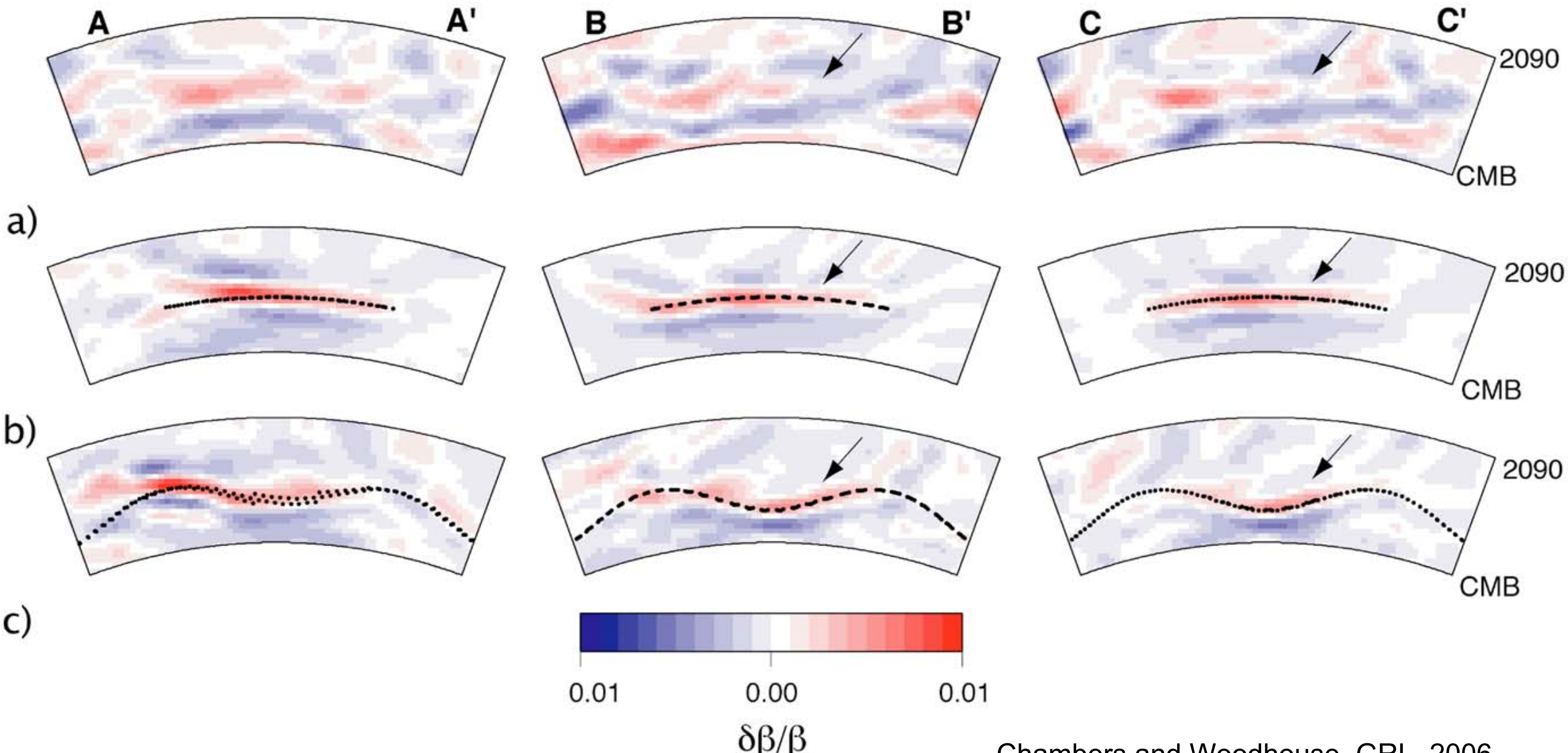

Chambers and Woodhouse, GRL. 2006

Comparison of migration results (black traces) with tomographic model S20RTS (coloour background, Ritsema, van Heijst and Woodhouse, 1999). The red line marks the inferred position of the D’’ discontinuity. In section A-A’ an elevation of the reflector coincides with a region of high velocity, while in B-B’ and C-C’ the reflector is restricted to a region of high velocity

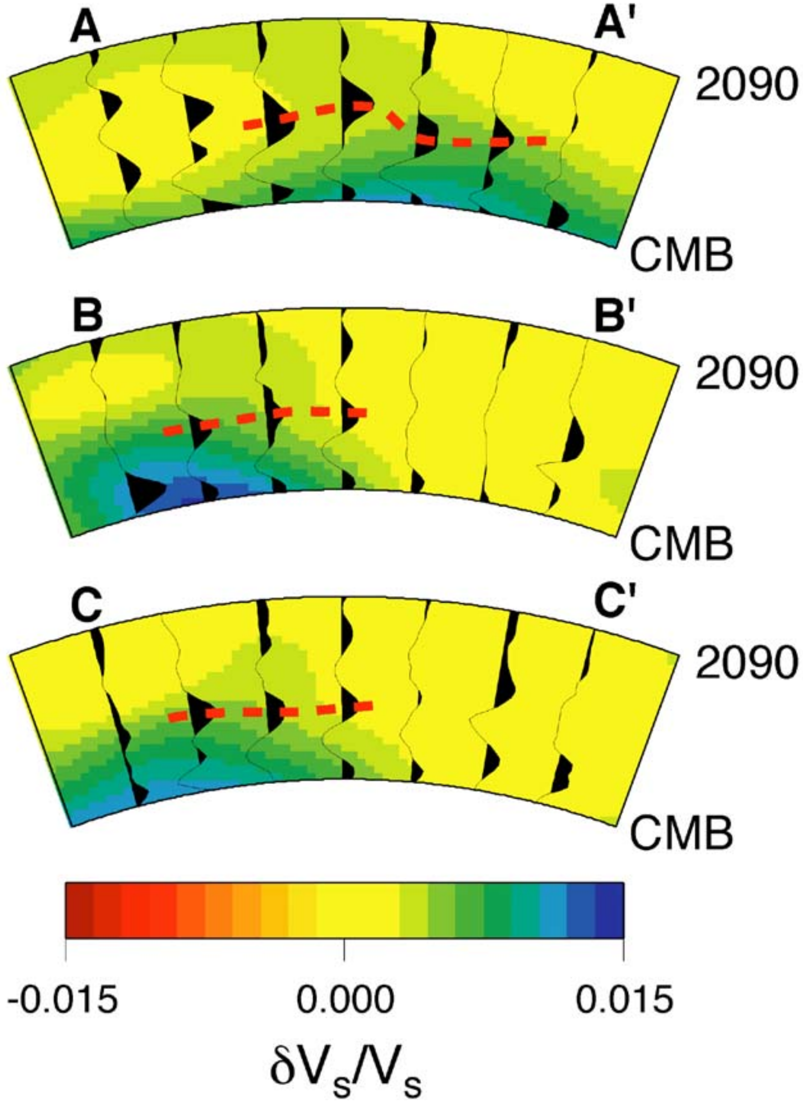

Chambers and Woodhouse, GRL, 2006

From Wookey et al, Nature, 2005

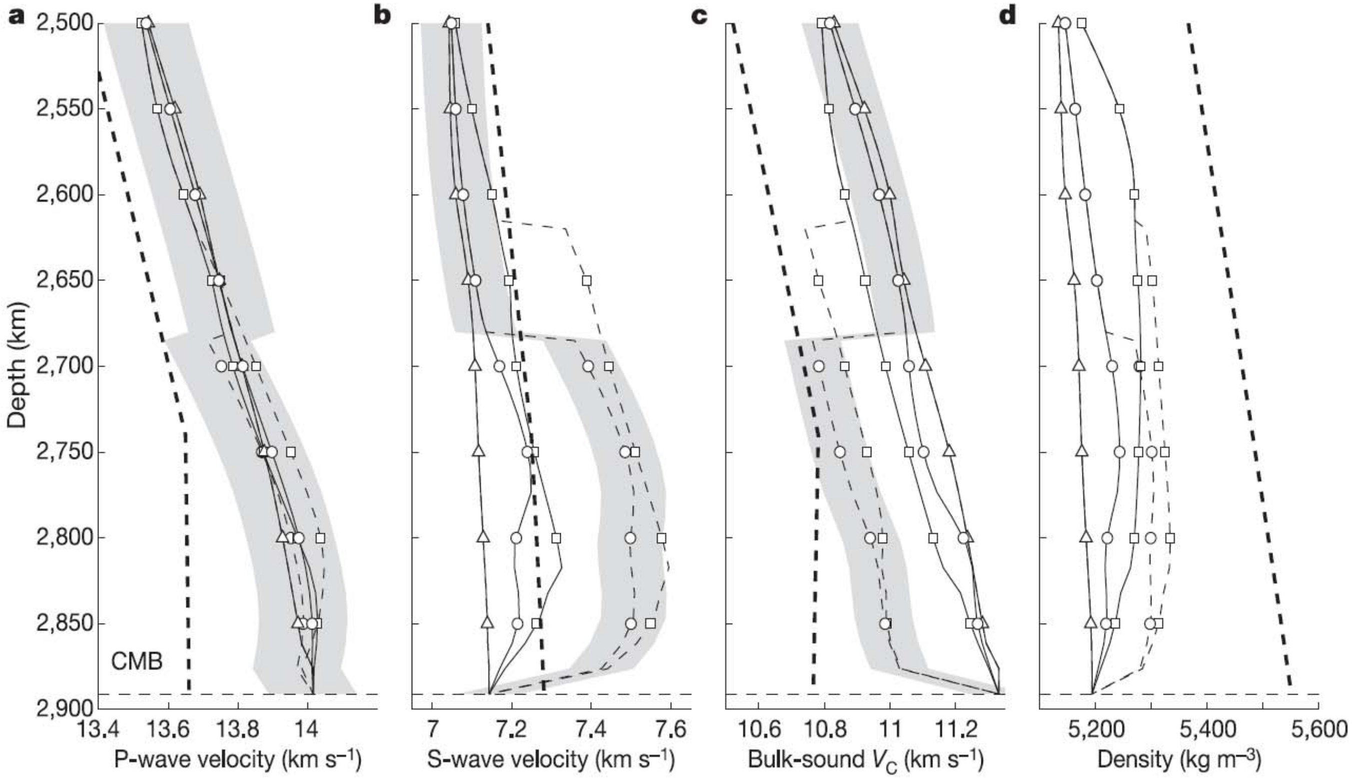

Figure 2 | **Seismic properties interpolated from *ab initio* calculations.** These show the P-wave (**a**) and S-wave (**b**) velocities, the bulk-sound speed (**c**) and the density (**d**) for the 'hot' (triangles), 'average' (circles) and 'cold' (squares) mantle convection profiles. These are converted from the temperature profiles in Fig. 1 into variation of the seismic properties with depth by interpolation of our *ab initio* results. The solid traces are the variation solely due to temperature (in perovskite), and the dashed lines are where a phase-transformation is included. The shaded area shows the estimated constraint for the average profile (other profiles are similarly constrained). For comparison the velocities and density from the reference model ak135 (ref. 15) are included (black dashed trace).

Deep reflectors in Indonesia

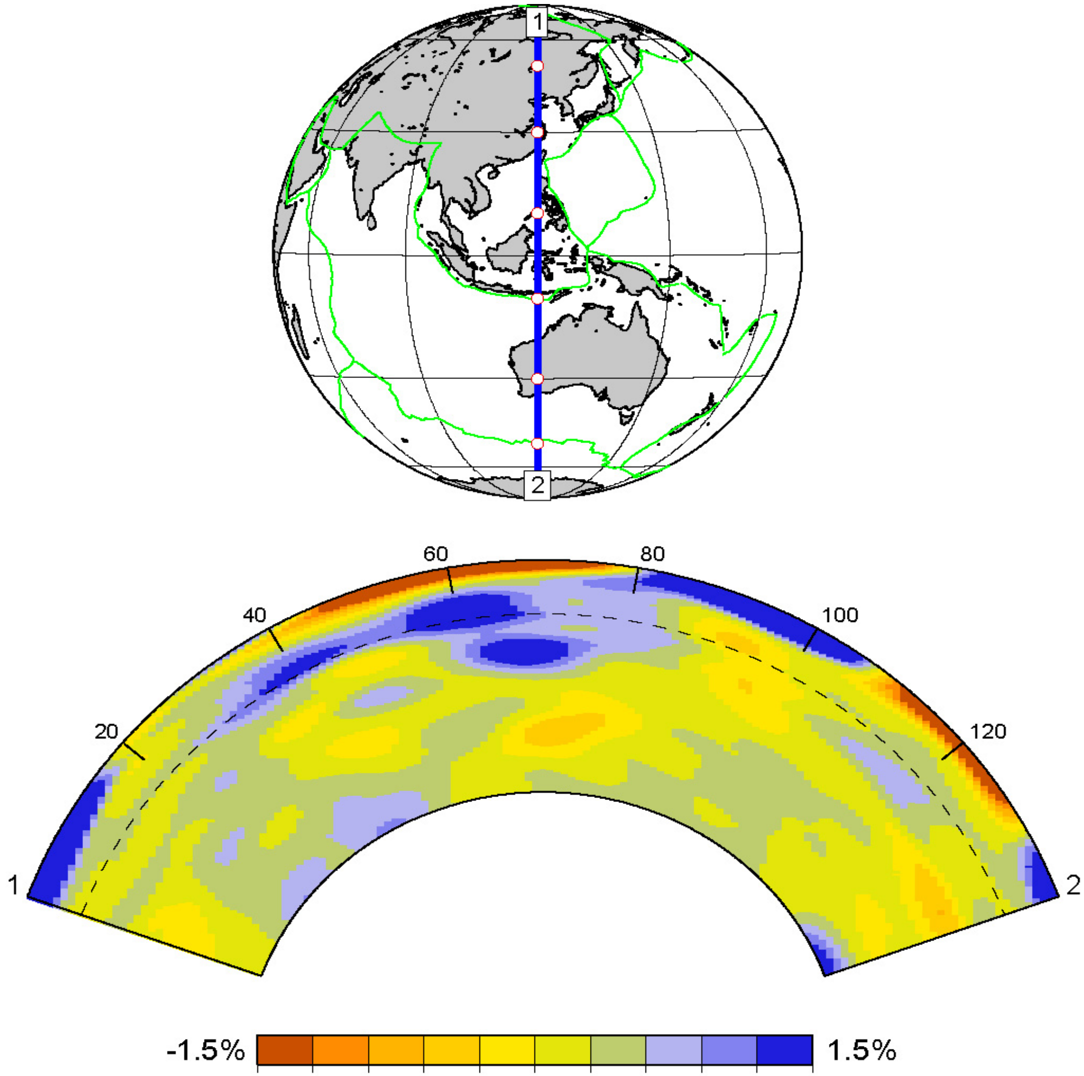

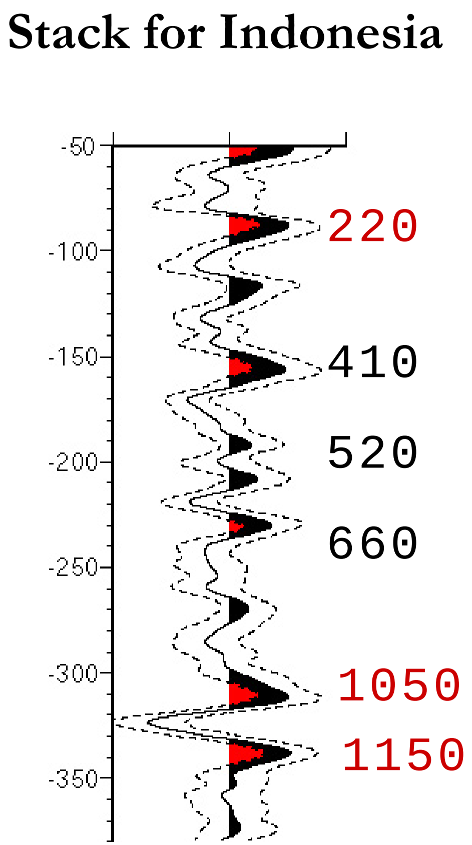

[*Deuss, DPhil Thesis 2002*]